Searching for a light Z' through Higgs production at the LHC

Frank F. Deppisch,[1,2,*] Suchita Kulkarni,[2,†] and Wei Liu[1,‡]

[1]*University College London, Gower Street, London WC1E 6BT, United Kingdom*
[2]*Institut für Hochenergiephysik, Österreichische Akademie der Wissenschaften, Nikolsdorfer Gasse 18, 1050 Wien, Austria*

(Received 25 September 2019; published 11 December 2019)

We investigate the potential of LHC resonance searches in leptonic final states to probe the Z' in the minimal $U(1)_{B-L}$ model. Considering the current constraints on the Z' in terms of its mass $m_{Z'}$ and the associated gauge coupling g_{B-L} as well as constraints in the Higgs sector, we analyze the potential of dilepton and four lepton final states for Z' production. This includes Drell-Yan production, Higgs mediated decays and final state radiation processes concentrating only on the ATLAS and CMS detectors at the LHC. We show that the four-lepton final state is sensitive to $m_{Z'}$ as low as 0.25 GeV. Furthermore, setting the Higgs mixing to $\sin\alpha = 0.3$, this final state has a strong sensitivity and it probes regions of parameter space where the Z' is long-lived. We demonstrate the sensitivity at the High Luminosity LHC and comment on the potential of probing displaced vertices due to long-lived Z'. Finally, we also comment on the strength of Z' and Higgs mediated heavy neutrino processes by taking into account the constraints derived.

DOI: 10.1103/PhysRevD.100.115023

I. INTRODUCTION

The presence of finite yet small tiny masses of neutrinos remains as one of the puzzles within the Standard Model (SM). Specifically, the ultimate goal is to determine the nature of neutrinos and the corresponding mechanism of neutrino mass generation. The mechanism is typically believed to be accompanied by the breaking of lepton number L symmetry resulting in a Majorana neutrino character. At the LHC and in other searches, it can be probed by searching for heavy neutrinos (or neutral heavy leptons, to use the other often used name) and other mediators of the different types of the seesaw mechanism. The difficulty to probe a parameter space relevant for light neutrino mass generation is often challenging due to the required lightness of neutrino; generically, this demands either heavy mediators (which may not be accessible at colliders) or small couplings to the SM neutrinos (which suppresses the mediator production rates). Other solutions exist, though, such as in inverse seesaw scenarios [1], where the suppression is achieved through a weakly broken lepton number symmetry or in radiative models with loop-suppressed neutrino masses.

Moreover, in the prominent seesaw type-I mechanism where three right-handed neutrinos N_i are added to the SM, the L symmetry breaking is explicit by assuming Majorana masses for the right-handed neutrinos. While this is perfectly valid as such masses for the gauge-sterile right-handed neutrinos are not forbidden by the SM gauge symmetry, the question of where the light neutrinos get their mass is simply shifted: where do the right-handed neutrinos get their masses? Clearly, the observable presence of the heavy sterile neutrinos provides the crucially testable consequence but embedding the seesaw mechanism in a more complete model will also provide additional means to probe the mechanism of neutrino mass generation. Arguably one of the simplest ultraviolet (UV) complete models for this purpose is described by the $U(1)_{B-L}$ extension of the SM gauge group [2,3], where particles are additionally charged under the quantum number $B-L$ (B is the usual SM baryon number). Here, three right-handed Majorana neutrinos are added as well, in order to give masses to the light neutrinos via seesaw type-I but also to cancel anomalies. The right-handed neutrino Majorana masses are generated by the spontaneous breaking of the $U(1)_{B-L}$ symmetry via an extra Higgs field χ.

The important prediction of this model is the presence of an additional gauge boson Z' associated with the $B-L$ gauge symmetry. The Z' can be probed for in several different ways. LHC searches for heavy resonance in dilepton final states put a strict bound on $m_{Z'} > 4.5$ TeV [4] for a g_{B-L} coupling similar to that of the SM Z boson.

*f.deppisch@ucl.ac.uk
†suchita.kulkarni@oeaw.ac.at
‡wei.liu.16@ucl.ac.uk

While the $B-L$ breaking scale $\langle\chi\rangle = m_{Z'}/(2g_{B-L})$ is constrained to be larger than 3.45 TeV from LEP-II [5–8], these limits are not applicable when $m_{Z'}$ becomes too small. Neutrino scattering experiments set an effective limit on $\langle\chi\rangle \gtrsim 1$ TeV [9–13]. The wider $m_{Z'} - g_{B-L}$ parameter space can, for example, be explored using the constraints on new theories using Rivet (CONTUR) method for $m_{Z'} \gtrsim 1$ GeV incorporating ATLAS and CMS results [14,15]. For $m_{Z'} < 10$ GeV limits are set at $g_{B-L} \lesssim 10^{-4}$ to 10^{-3} from recasting dark photon searches at LHCb using Darkcast [16]. For even smaller $m_{Z'} < 1$ GeV, proton and electron beam dump experiments are sensitive to long-lived Z' for sufficiently small $g_{B-L} \sim 10^{-8} - 10^{-4}$ [16]; cf. our summary Fig. 9.

Despite intense efforts to constrain new resonances at colliders, within the $B-L$ model, the parameter space of Z' masses between 1 to 100 GeV remains relatively unconstrained for $g_{B-L} < 10^{-3}$ [16]. In this work, we concentrate on this parameter space and analyze the reach of existing searches in leptonic final states at the ATLAS and CMS detectors. For masses less than 10 GeV, the factorization theorem is no longer applicable and the production should be dealt with via, e.g., the vector dominance mechanism. An alternative way to look for low mass Z' is to explore their production via heavier resonances. For the $B-L$ model this could be production via the $B-L$ Higgs or the SM Higgs. As we will demonstrate later, the $B-L$ Higgs is not a good production channel; however, Z' production via the SM Higgs remains a viable option. Recently this production mechanism is under attention as one of the key processes to explore dark photon models at the LHC. Because of new developments in analysis strategies, dark photon masses as low as 0.25 GeV are constrained. This motivates analysis of $B-L$ models in the same final state and understanding the reach of these searches. Above the mass of 10 GeV, the resonance searches in, e.g., dilepton final states will prove to be useful. Currently, the best limits in this region are obtained via the LHCb search for dark photons [17].

Z' production via SM Higgs as will be explored in this work is, however, dependent on the mixing angle between the $B-L$ Higgs and the SM Higgs. This production mechanism is therefore subject to constraints on the Higgs sector from both direct and indirect searches [18–35]. These limit the $B-L$ Higgs–SM Higgs mixing angle and therefore the strength of the Z' production at the LHC. Current constraints on the Higgs mixing angle include those from direct searches for additional Higgs bosons at the LHC, the SM Higgs signal strength measurements, as well as constraints from electroweak observables and the measurements of the W mass. They are further complemented by constraints from theoretical considerations of the perturbativity of the Higgs couplings, unitarity, and vacuum stability.

In this work, we explore three different Z' production mechanisms and derive limits for low mass Z'. The first process we consider is $pp \to Z' \to \mu^+\mu^-$. We refer to this as the Drell-Yan Z' production channel. Second, we consider the final state radiation of Z'. Here the Z' is radiated off via the muons in decay products of SM Z. More precisely, the process is $pp \to Z \to \mu^+\mu^- Z' \to 4\mu$. Finally, we consider the Z' production via the SM Higgs portal with Z' decays to leptonic final state $pp \to h \to Z'Z' \to 4l$. In combining these three processes, we derive new constraints in the $m_{Z'}$–g_{B-L} parameter space of the minimal $U(1)_{B-L}$ model.

As it will turn out, the Z' will be long-lived for masses $m_{Z'} \lesssim 1$ GeV and $g_{B-L} \lesssim 10^{-5}$. At the LHC, this lifetime frontier can be explored via displaced signatures. This region is of particular interest for Higgs mediated Z' production. Because of the large mass difference between the SM Higgs and the Z', the Z' receives a large boost leading to macroscopic lab frame displacement and displaced vertices can be observed. We will carefully chalk out the regions where Z' is displaced and demonstrate the potential of existing searches.

The plan of the paper is as follows: In Sec. II, we briefly review the minimal $B-L$ model and its parameter space under consideration. Section III contains a discussion of the associated collider signatures, whereas Sec. IV is devoted to a discussion of the LHC searches we incorporate in our analysis. We derive limits in Sec. V, and Sec. VI concludes our work.

II. THE MINIMAL $U(1)_{B-L}$ MODEL

A. Model setup

The minimal $U(1)_{B-L}$ was first described in Ref. [3]. We here discuss the salient features as far as relevant for our discussion. In addition to the particle content of the SM, the $U(1)_{B-L}$ model incorporates an Abelian gauge field B'_μ, a SM singlet scalar field χ and three right handed neutrinos (RH neutrinos) N_i. The gauge group is $SU(3)_C \times SU(2)_L \times U(1)_Y \times U(1)_{B-L}$, where χ and N_i have $B-L$ charges $B-L = +2$ and -1, respectively. The SM fermions have $B-L$ charges determined by their usual baryon B and lepton L numbers, whereas all other SM fields are uncharged under $U(1)_{B-L}$. This fully describes the gauge sector of the model, where we make the assumption that the mixing between the $U(1)_{B-L}$ and $U(1)_Y$ fields vanishes. Even though this kinetic mixing arises naturally in loop diagrams, as it is scale dependent, we assume it to be zero at the electroweak scale, and the value at other scales can be derived from the renormalization group evolution; cf. Ref. [36] for a similar example. This assumption is made as a simplification to analyze the interplay between the Higgs mixing and the $U(1)_{B-L}$ gauge coupling.

The scalar sector is uniquely determined by the scalar potential

$$\mathcal{V}(H,\chi) = m^2 H^\dagger H + \mu^2|\chi|^2 + \lambda_1 (H^\dagger H)^2 + \lambda_2|\chi|^4 + \lambda_3 H^\dagger H|\chi|^2, \tag{2.1}$$

incorporating all allowed terms for the SM Higgs doublet H and the new scalar field χ. The breaking of the $(B-L)$ symmetry is achieved spontaneously such that χ acquires a vacuum expectation value (VEV) $\langle\chi\rangle$ breaking $SU(3)_C \times SU(2)_L \times U(1)_Y \times U(1)_{B-L} \to SU(3)_C \times SU(2)_L \times U(1)_Y$ above the electroweak (EW) scale. Consequently, the $U(1)_{B-L}$ gauge field acquires a mass

$$m_{Z'} = 2 g_{B-L} \langle\chi\rangle. \tag{2.2}$$

Likewise, the $U(1)_{B-L}$ and EW breaking will generate a mixing between χ and the SM Higgs through the λ_3 term in Eq. (2.1). Specifically, the mass matrix of the Higgs fields (H,χ) at tree level is [35]

$$M_h^2 = \begin{pmatrix} 2\lambda_1 v^2 & \lambda_3 x v \\ \lambda_3 x v & 2\lambda_2 x^2 \end{pmatrix}, \tag{2.3}$$

with $x = \langle\chi\rangle$ and $v = \langle H_0\rangle$, resulting in the mass eigenstates h, h_χ with masses

$$m^2_{h(h_\chi)} = \lambda_1 v^2 + \lambda_2 x^2 - (+)\sqrt{(\lambda_1 v^2 - \lambda_2 x^2)^2 + (\lambda_3 x v)^2}. \tag{2.4}$$

Here we assume that the SM-like Higgs h is lighter than the exotic Higgs $h_\chi \sim \chi$, and the physical Higgs states (h, h_χ) are related to the gauge states (H, χ) as

$$\begin{pmatrix} h \\ h_\chi \end{pmatrix} = \begin{pmatrix} \cos\alpha & -\sin\alpha \\ \sin\alpha & \cos\alpha \end{pmatrix} \begin{pmatrix} H \\ \chi \end{pmatrix}. \tag{2.5}$$

Here, α is the mixing angle relating the two bases. At tree level it can be computed from the parameters in the scalar potential and the scalar VEVs as

$$\tan(2\alpha) = \frac{\lambda_3 v x}{\lambda_2 x^2 - \lambda_1 v^2}. \tag{2.6}$$

While we do not discuss heavy neutrinos explicitly in this paper, we include for completeness how the seesaw type-I mechanism is naturally embedded in this model. Because of the charge assignments $(B-L) = -1$ for the right-handed neutrinos N_i and $(B-L) = +2$ for the scalar χ, the following two Yukawa-type interactions are allowed by the model gauge group,

$$\mathcal{L} \supset -y^\nu_{ij} \overline{L_i} \nu_{Rj} \tilde{H} - y^M_{ij} \overline{\nu^c_{Ri}} \nu_{Rj} \chi + \text{H.c.} \tag{2.7}$$

Here, L_i are the SM lepton doublets, $\tilde{H} = i\sigma^2 H^*$, and a summation over the generation indices $i, j = 1, 2, 3$ is implied. The Yukawa matrices y^ν and y^M are *a priori* arbitrary; the RH neutrino mass is generated due to breaking of the $B-L$ symmetry, with the mass matrix given by $M_R = y^M \langle\chi\rangle$. The light neutrinos mix with the RH neutrinos via the Dirac mass matrix $m_D = y^\nu v/\sqrt{2}$. The complete mass matrix in the (ν_L, ν_R) basis is then

$$\mathcal{M} = \begin{pmatrix} 0 & m_D \\ m_D & M_R \end{pmatrix}. \tag{2.8}$$

In the seesaw limit, $M_R \gg m_D$, the light and heavy neutrino masses are $m_\nu = -m_D M_R^{-1} m_D^T$ and $m_N = M_R$, respectively. Considering a simple one-generational scenario, this leads to the celebrated seesaw mechanism which induces a mixing between the light and heavy neutrinos,

$$\begin{pmatrix} \nu_L \\ \nu_R^c \end{pmatrix} \approx \begin{pmatrix} 1 & -\theta_\nu \\ \theta_\nu & 1 \end{pmatrix} \begin{pmatrix} \nu \\ N \end{pmatrix}, \tag{2.9}$$

with the small mixing angle $\theta_\nu = \sqrt{m_\nu/m_N}$. For $m_\nu \approx 0.1$ eV and $m_N \approx 10$ GeV this gives a very small mixing angle $\theta_\nu \approx 3 \times 10^{-6}$. With these choices of parameters, one can compute the Yukawa couplings for the light and heavy neutrinos, $y^M = m_N/\langle\chi\rangle \approx 10^{-3}$, and $y^\nu \approx \sqrt{m_N m_\nu}/v \approx 10^{-7}$. Considering only SM gauge interactions, heavy neutrino production rates via the SM W and Z will be suppressed by θ_ν^2. In the $(B-L)$ model considered here, the heavy neutrinos are also produced via Z' and χ. It is therefore important to probe these exotic particles as stringently as possible to learn about the viability of neutrino mass generation mechanisms near the EW scale.

B. Constraints on the parameter space

The main focus of this work is to explore the viability of producing Z' through the SM Higgs. In this context, we are specifically interested in three model parameters: the Z' mass $m_{Z'}$, the $U(1)_{B-L}$ gauge coupling g_{B-L}, and the Higgs mixing angle parametrized as $\sin\alpha$. As already stated, we assume that the mixing of the Z' with the SM Z vanishes, and we implicitly consider the second Higgs h_χ to be heavy enough so as not to affect our calculations.

Neutral gauge bosons, such as the Z' in our model, have been searched for in numerous experiments. As the Z' couples to quarks and leptons at tree level, it can be searched for via the s-channel production at various colliders. Several such searches exist at, e.g., KLOE [37], *BABAR* [38], and the LHC [17]. Resonance searches at the LHC for additional gauge bosons in dilepton final states currently rule out Z' masses up to approximately 4 TeV [39,40]. These searches, however, are limited in their ability to search for Z' below a 100 GeV due to large event rates at the LHC. Complementary searches in dijet final states probe lower masses up to 10 GeV [41]. However, the limits from these searches are weak. For Z' masses below 100 GeV, the most relevant limits arise from low energy colliders, from fixed target experiments, and from electroweak precision tests. Among colliders, *BABAR* reaches the lowest Z' mass of 0.05 GeV, up to 10 GeV of Z' mass, the

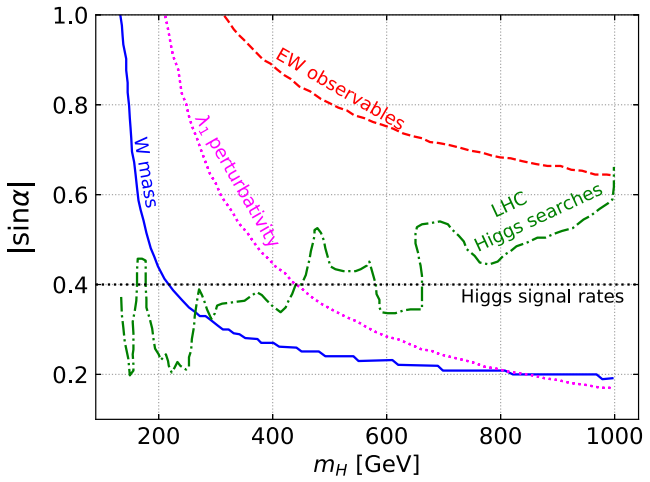

FIG. 1. Summary of constraints on the Higgs mixing angle $|\sin\alpha|$ as a function of the mass m_H of the additional Higgs for a fixed value of $\tan\beta = v/\langle\chi\rangle = 0.1$. As indicated, the constraints arise from theoretical considerations of perturbativity (dotted magenta curve), indirect experimental constraints from corrections to the W boson mass (solid blue curve), electroweak precision observables (dashed red curve), direct LHC searches for additional Higgs bosons (dash-dotted green curve), and LHC measurements of the Higgs signal rates (dotted black line). The plot is adapted from [19].

limit of g_{B-L} is approximately constant at 10^{-4}. For Z' mass between 10 and 70 GeV, the strongest limits are placed by LHCb and they constrain $g_{B-L} < 10^{-3}$. For light Z' below 1 GeV, there are stronger limits from fixed target experiments; however, this region is not of primary interest to this work.

The other relevant sector for us is that of the Higgs. The singlet scalar χ and its mixing angle $\sin\alpha$ with the SM Higgs can be constrained in various ways. From theoretical consistency arguments, perturbativity, unitarity, and vacuum stability requirements set limits on the quartic couplings of the Higgs sector. The current constraints on the Higgs mixing angle $|\sin\alpha|$ as a function of the heavy Higgs mass and for a fixed value of $v/\langle\chi\rangle = 0.1$ is taken from Ref. [19] and is summarized in Fig. 1. Direct limits from the Higgs signal strength measurements put a global upper limit of $|\sin\alpha| \lesssim 0.4$ [18–28], independent of the mass of the heavy Higgs. The LHC searches for additional Higgs bosons tightly constrain the presence of extra Higgses with masses below $m_H = 300$ GeV. Above the mass of 300 GeV, the strongest limits are obtained by considering corrections to the W mass, and they limit the mixing angle at $|\sin\alpha| < 0.3$ for a heavy Higgs mass of 300 GeV. The constraint gets tighter as the heavy Higgs mass increases and in the limiting case of Higgs mass of 1 TeV, the limit approaches $|\sin\alpha| \lesssim 0.2$. For such large heavy Higgs masses, however, the perturbativity of the λ coupling gives a similar constraint on $|\sin\alpha|$. Consequently, we take the Higgs mixing up to its maximally allowed value $|\sin\alpha| = 0.3$ combining the allowed region near $m_{h_\chi} \approx 300$ GeV mainly from the strong limits from the W boson mass and the direct Higgs searches. It is important to note that the limit on $|\sin\alpha|$ gets only mildly stronger for heavier Higgs masses. In the future, the limit on the Higgs mixing could be improved considerably to $\sin\alpha \lesssim 0.06$ at a lepton collider such as CEPC [42,43] or the FCC-ee [42].

C. Z' decays

Another important quantity for this work is the Z' decay length. The decay length in general is a function of the Z' mass and the g_{B-L} coupling. As g_{B-L} decreases, it is possible for Z' to obtain macroscopic decay lengths. The total decay width of Z' can be approximately expressed as

$$\Gamma(Z') \approx \frac{23}{9}\frac{g_{B-L}^2}{4\pi} m_{Z'}, \tag{2.10}$$

for $m_{Z'} \gtrsim 2m_\mu$ and neglecting the effect of QCD resonances. It gives rise to an approximate Z' proper decay length of

$$L_0 \approx 1\ \text{mm} \cdot \left(\frac{10^{-6}}{g_{B-L}}\right)^2 \cdot \left(\frac{1\ \text{GeV}}{m_{Z'}}\right). \tag{2.11}$$

For small Z' masses $m_{Z'} \lesssim 1$ GeV the leading order Z' branching ratio computation as done by MadGraph may not be accurate and nonperturbative QCD effects become important. These effects are accounted for by scaling the branching ratio to the corresponding results obtained by the Darkcast calculation. Darkcast considers these effects by means of the vector meson dominance mechanism [44]. As the $B-L$ model in Darkcast does not contain heavy neutrinos, three degenerate heavy neutrinos are also added to model accurately the branching ratio computation.

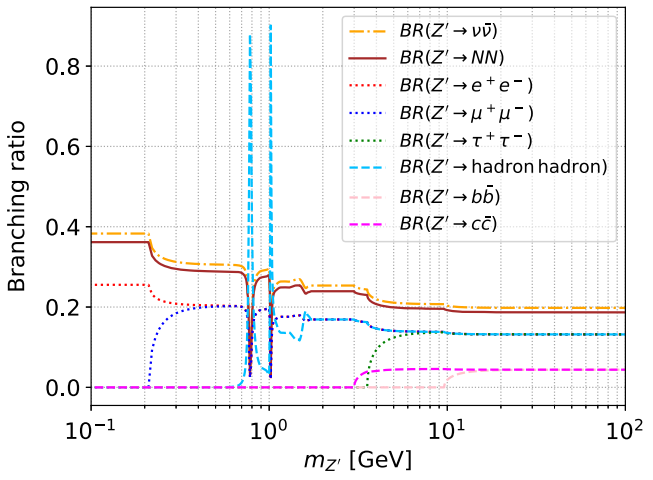

FIG. 2. Z' branching ratio to various final states as a function of the Z' mass. The mass of the three heavy degenerate neutrinos N_i in the model is fixed to $m_N = m_{Z'}/3$.

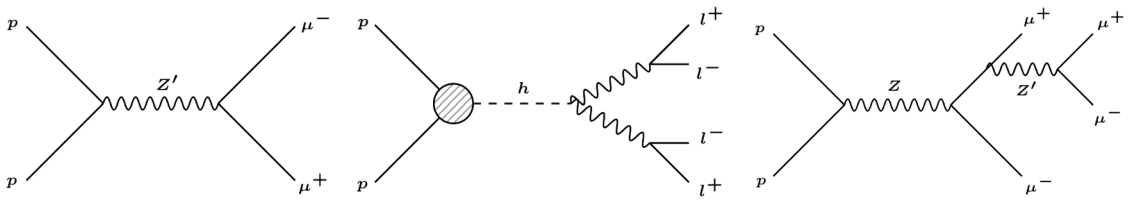

FIG. 3. Feynman diagrams of Z' production modes considered in this paper: Drell-Yan Z' s-channel $pp \to Z' \to \mu^+\mu^-$ (left), Z' pair production via SM Higgs $pp \to h \to Z'Z' \to 4\mu$ (center), and Z' final state radiation from SM Z $pp \to Z \to Z'\mu^+\mu^- \to 4\mu$ (right).

In Fig. 2, we plot the Z' branching ratios to the SM states and the heavy neutrinos. The model contains three heavy neutrinos which we choose to be degenerate at a mass of $m_N = m_{Z'}/3$. This maximizes the branching ratio to neutrinos and minimizes that to muons, making it a conservative choice for our analysis, although the effect is in any case small. Beyond a Z' mass of 1 GeV the branching ratios approximately remain constant with the exception of $\tau\tau$, $c\bar{c}$, and $b\bar{b}$ having thresholds at 3.0, 3.4, and 9.6 GeV, respectively. For Z' masses below 1 GeV several thresholds due to QCD hadrons are visible. Effects due to loop corrections are accounted for as described before. Of particular importance for this work is the $\mathrm{BR}(Z' \to l^+l^-)$, which is approximately constant at 15% per lepton species.

III. Z' PRODUCTION MECHANISMS

A potentially large Higgs mixing angle of order $\sin\alpha \approx 0.3$ implies that it is possible to produce the Z' via decays of the SM Higgs. This presents an alternative and interesting possibility to probe the Z' which is usually searched for via s-channel Drell-Yan production mode; cf. Fig. 3 (left). In the Higgs mediated case, Fig. 3 (center), the production is through a different vertex driven by the Higgs mixing $\sin\alpha$ but $m_{Z'}$ is restricted to $m_{Z'} < m_h/2 \approx 62$ GeV. Alternatively, it is also possible to produce the Z' via final state radiation in the Drell-Yan Z production at the LHC; cf. Fig. 3 (right).

With these observations, we will concentrate on three distinct processes at the LHC: Drell-Yan Z' production, Z' pair production through SM Higgs, and final state radiation (FSR) of Z' in the Drell-Yan production of a SM Z. We concentrate on leptonic final states. In particular, we analyze the reach of following LHC analyses for the given final states

(i) $pp \to Z' \to \mu^+\mu^-$ [45],
(ii) $pp \to h \to Z'Z' \to 4\mu$ [46], $\to 4\ell$ [47],
(iii) $pp \to Z \to \mu^+\mu^- Z' \to 4\mu$ [48].

Apart from the above processes, it is also possible to search for Z' via associated production with W/Z or a jet. These processes will, however, yield a smaller production cross section compared to the ones listed above. Therefore, we will not explicitly consider them in this work. The associated production is accounted for in the s-channel production of Z' in the form of showering and hadronization. As mentioned before, numerous resonance search results in dijet final states are also available. Their limits are, however, weak, and therefore, we do not consider hadronic searches in this work.

Before proceeding with a detailed collider analysis of the above processes, it is instructive to take a look at the production cross sections and branching ratios relevant in each channel.

A. Drell-Yan Z' production

The Z' can be directly generated via pp collisions at the LHC through s-channel Drell-Yan production. The cross section is a function of g_{B-L} and $m_{Z'}$. For $g_{B-L} = 10^{-3}$, the production cross section varies from several picobarn for light Z' around 10 GeV to $\mathcal{O}(100)$ fb for a Z' mass of 100 GeV. Figure 4 (top left) illustrates the dependence of the cross section on g_{B-L} and $m_{Z'}$. The cross section falls by 2 orders of magnitude for every order of magnitude change in g_{B-L}. We also overlay a contour showing the proper Z' displacement of 1 mm (dashed red line). It is clear that it will be difficult to probe large regions of displaced Z' via Drell-Yan production as the Z' cross section becomes very small for small g_{B-L}. The cross section is only calculated for $m_{Z'}$ greater than ≈ 10 GeV to avoid nonperturbative effects. Although the Z' production cross section is very large for small masses, it becomes increasingly challenging to search for such a light mass Z' at the LHC as both the signal and background event rates become too high. The limitations on the search due to trigger rates can be circumvented by means of data scouting techniques or trigger level analyses. We will demonstrate below the reach of a recent scouting analysis on low mass Z'.

B. Z' pair production via SM Higgs

When $m_{Z'} < m_h/2$, the exotic gauge boson Z' can be pair produced via the SM-like Higgs h. We assume $m_{h_\chi} > m_h$ and thus the mostly exotic Higgs h_χ does not play a role in the process. If the Higgs mixing angle is at its currently allowed value, $\sin\alpha \approx 0.3$, the process $pp \to h \to Z'Z'$ can produce Z' efficiently,

$$\begin{aligned}\sigma(pp \to h \to Z'Z') &= \sigma(pp \to h) \times \mathrm{BR}(h \to Z'Z') \\ &= \cos^2\alpha \times \sigma(pp \to h_{\mathrm{SM}}) \frac{\Gamma(h \to Z'Z')}{\cos^2\alpha\,\Gamma(h_{\mathrm{SM}}) + \Gamma(h \to Z'Z')},\end{aligned} \tag{3.1}$$

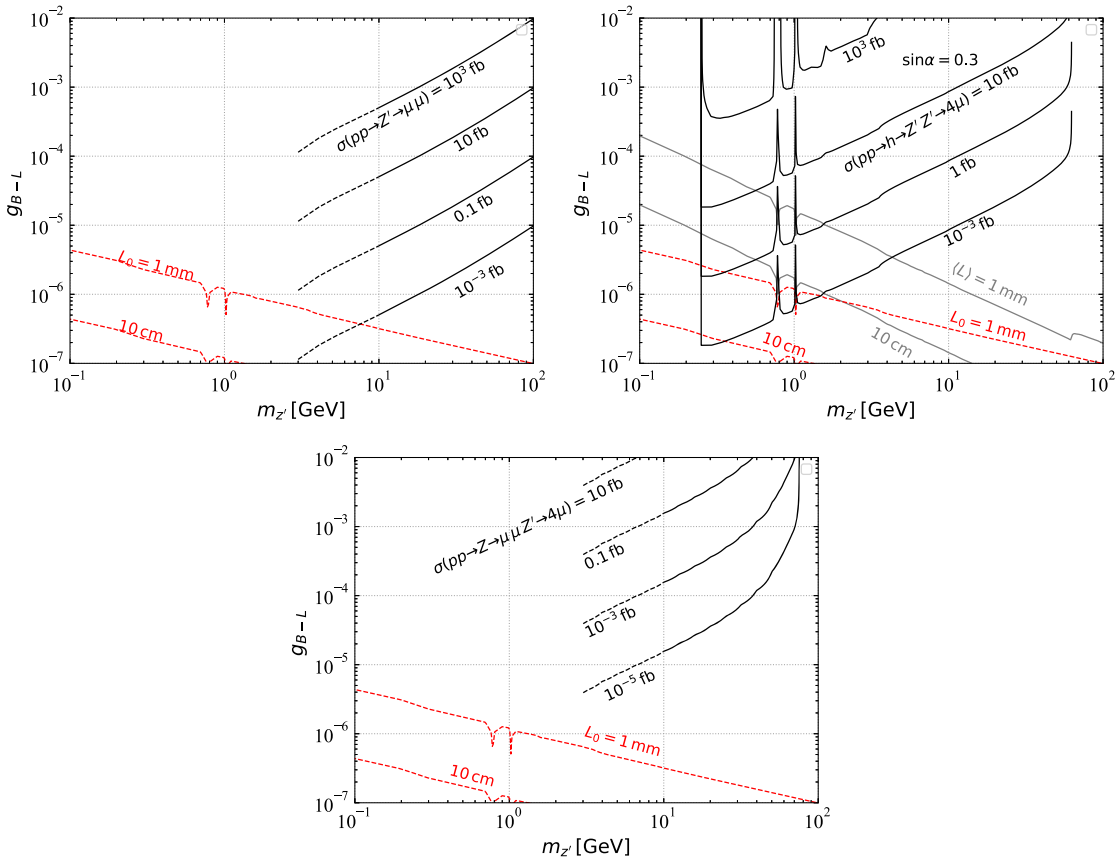

FIG. 4. Cross section of Drell-Yan Z' production, $pp \to Z' \to \mu^+\mu^-$ (top left), Z' pair-production via Higgs, $pp \to h \to Z'Z' \to 4\mu$ (top right), and Z production with FSR, $pp \to Z \to 2\mu + Z' \to 4\mu$ (bottom), as a function of the Z' mass $m_{Z'}$ and the $U(1)_{B-L}$ gauge coupling g_{B-L} (black solid curves). All cross sections are at 13 TeV. In the upper right plot, the Higgs mixing is set to $\sin\alpha = 0.3$. The red lines represent the proper decay length L_0 of the Z' as indicated, whereas the blue lines in the upper right plot indicate the average Z' lab frame displacement $\langle L\rangle$ as it is produced via the SM Higgs.

where $\sigma(pp \to h_{\rm SM}) \approx 44 \pm 4$ pb is the pure SM Higgs production cross section at 13 TeV [49] and $\Gamma(h_{\rm SM}) \approx 4$ MeV is the total Higgs width in the SM [50]. In Eq. (3.1), we neglect the small partial width of the Higgs decaying to heavy neutrinos, $\Gamma(h \to NN)$, when calculating the total width [51]. The partial decay width to $Z'Z'$ is in our model given by

$$\Gamma(h \to Z'Z') = \frac{3g_{B-L}^2 \sin^2\alpha}{8\pi m_{Z'}^2} m_h^3 \sqrt{1 - \left(\frac{2m_{Z'}}{m_h}\right)^2} \times \left(1 - 4\left(\frac{m_{Z'}}{m_h}\right)^2 + 12\left(\frac{m_{Z'}}{m_h}\right)^4\right). \quad (3.2)$$

The cross section in Eq. (3.1) is shown in Fig. 4 (top right) as a function of $m_{Z'}$ and g_{B-L}, where the Higgs mixing is set to $\sin\alpha = 0.3$. Also superimposed are contours of constant proper Z' decay length L_0 in the rest frame and the average decay length $\langle L\rangle$ in the lab frame at 1 mm and 10 cm. The proper and average lab frame displacements are very different for lighter Z' due to the associated boost. It can also be seen that Z' starts to be appreciably displaced with $\langle L\rangle = 1$ mm for this production mode for $g_{B-L} \approx 10^{-4}$ when $m_{Z'}$ is less than a giga-electron-volt. As $m_{Z'}$ increases, small values of g_{B-L} are required to gain the

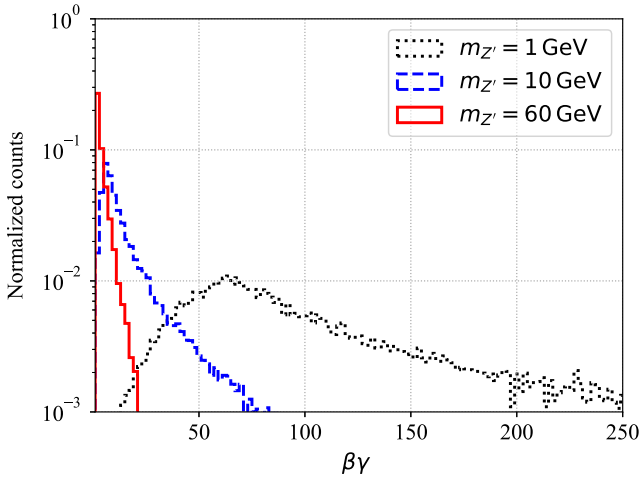

FIG. 5. Truth level distribution of the Z' boost factor $\beta\gamma$ in Z' pair production via SM Higgs, $pp \to h \to Z'Z'$.

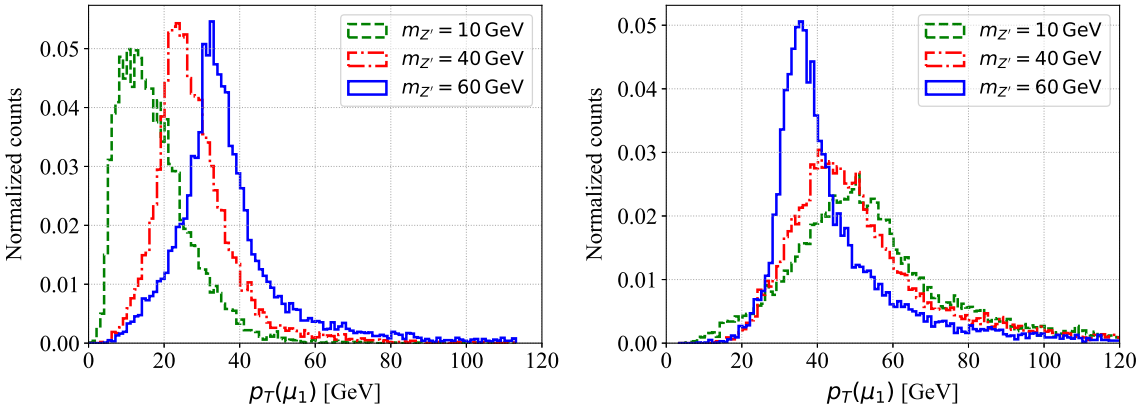

FIG. 6. Truth level distribution of the transverse momentum of the leading muon for the Higgs production mode $pp \to h \to Z'Z' \to 4\mu$ (left) and the FSR mode $pp \to Z \to Z'\mu^+\mu^- \to 4\mu$ (right), for three different values of $m_{Z'}$.

same displacement. At this point, however, the Higgs mediated Z' production cross section is very small.

To better understand the Z' boost and corresponding Z' lab decay length, we show in Fig. 5 the distribution for the boost factor $\beta\gamma = |\mathbf{p}_{Z'}|/m_{Z'}$ for different $m_{Z'}$ ranging from 1 to 60 GeV. For a light Z' with $m_{Z'} = 1$ GeV, typical boost factors can reach beyond 100 but this decreases steadily for heavier Z' and for $m_{Z'} = 60$ GeV, $\langle\beta\gamma\rangle$ is of order unity. For large $\beta\gamma$ the lab frame displacement can be very large even if the proper decay length is microscopic. At the LHC, however, it will be difficult to probe a large region of the parameter space as the $hZ'Z'$ coupling is also proportional to g_{B-L}. Therefore, a small value of g_{B-L} leads to a small production cross section. As we will discuss later, this interplay of boost, corresponding lab frame decay length, and suppression of production cross section lead to interesting results.

Along with the estimates of the total cross section it is imperative to gain an understanding of the broad kinematics of the processes we are considering. To this extent, in Fig. 6 (left) we plot the p_T distribution of the final state leading muon for Higgs mediated Z' production. The p_T of the leading muon increases as the mass of Z' increases. This is to be expected as the Higgs is produced almost at rest and the muon p_T is controlled by the Z' mass.

C. Z' final state radiation from Z production

In the context of LHC analyses, the production of a Z' radiating from a lepton is particularly useful to explore in models, such as that based on $L_\mu - L_\tau$, where it is not possible to produce the associated Z' from quark annihilation. In the case of the $B-L$ Z' this is not really necessary; however, for completeness we discuss this process and show the total cross section as well as later determine the resulting constraints from this channel. As shown in Fig. 4 (bottom), the overall production cross section of this process is rather small as an emission of a massive particle from final state muon requires the muon to be off-shell and hence it is phase space suppressed. The cross section is only calculated for $m_{Z'}$ greater than 10 GeV to avoid nonperturbative effects. The cross section attains a maximal value of 1 fb in the considered parameter space for $g_{B-L} < 10^{-3}$. In the leading muon p_T distribution,[1] Fig. 6 (right) for this process, the dependence on $m_{Z'}$ is reversed to that for the Higgs production. This is understood because the overall energy momentum of the process is conserved. Therefore, to produce a more and more massive gauge boson in the final state, the muons are required to be softer.

IV. RECASTING PROCEDURE

In this section, we explain our recasting procedures for the existing ATLAS/CMS searches so that we can apply them to the $B-L$ model considered here. Either we exploit model-independent limits given by the collaborations or we use event simulations to calculate the corresponding fiducial cross section in the $B-L$ model which we then compare with the experimental limit.

We use the Universal FeynRules Output (UFO) [52] for the $B-L$ model with next-to-leading order (NLO) QCD production, developed in Ref. [51], in combination with the Monte Carlo event generator MadGraph5AMC@NLO-v2.6.3 [53] at parton level. For every signal sample, we generate 10^4 signal events. We then pass the generated parton level events to PYTHIA v8.235 [54] which handles the initial and final state parton showering, hadronization, and heavy hadron decays. We do not simulate detector effects. Individual analysis efficiencies as described later are taken into account in order to obtain results. The analysis results we consider here include either fiducial cross sections reported in a certain part of the phase space without detector effects or experimental efficiencies which can be applied to hadronized events. We therefore do not compromise on the accuracy of our results due to the

[1]No interference effects with the SM Z are taken into account at this point.

absence of a detector simulation. For the Higgs-mediated mode we use the NLO capabilities of our model to simulate Higgs production via gluon-gluon fusion.

Z' pair production via SM Higgs at CMS (CMS $h \to 4\mu$). In Ref. [46], the CMS Collaboration reported on a search for the pair production of new light bosons decaying into muons at $\sqrt{s} = 13$ TeV with an integrated luminosity of 35.9 fb^{-1}. The search was optimized for prompt exotic boson decays as well as those with moderate displacements. As results of the search, upper limits on the signal cross sections in prompt final state are presented for neutral boson masses between 0.25 and 3.55 GeV, or approximately $2m_\mu$ and $2m_\tau$. However, the analysis is valid for a dimuon invariant mass up to ≈9 GeV. We therefore reimplement the analysis and derive limits for $m_{Z'}$ up to 8.5 GeV. In order to achieve this, we use model-independent upper limits on the signal cross sections presented in the analysis. To derive the theory predictions, the analysis reports that the detector efficiency $\epsilon_{\text{detector}}$ is almost independent of the signal model. This has been demonstrated in the analysis by taking the ratio of the generator level acceptance α_{gen} with the total efficiency for several signal samples. This factor, $\epsilon_{\text{detector}} = \alpha_{\text{gen}}/\epsilon_{\text{total}}$, is approximately constant and reported to be 60%. In order to assist simulating α_{gen}, the analysis advocates applying the cuts

$$\begin{aligned} &p_T(\mu_1) > 17 \text{ GeV}, \\ &\quad |\eta| < 0.9, \qquad \text{for the leading muon}, \\ &p_T(\mu) > 8 \text{ GeV}, \\ &\quad |\eta| < 2.4, \qquad \text{for the other three muons}. \end{aligned} \tag{4.1}$$

In addition, transverse, L_{xy}, and lateral, L_z, displacements of each muon from the interaction point are required to be

$$L_{xy} < 9.8 \text{ cm}, \qquad L_z < 46.5 \text{ cm}, \tag{4.2}$$

so, in fact, the selection criteria include scenarios where the Z' can be appreciably long-lived with $L_0 \lesssim 10$ cm.

We have verified the reported α_{gen} by producing a sample of SM Higgs decaying to light Z' of 1 GeV and applying the cuts as reported above. For our model, the cuts on the L_{xy} or L_z are not relevant in most of the parameter space as the Z' is not long-lived. Nevertheless, for light Z' with small g_{B-L} the decay length in the lab frame can be macroscopic. For example, for $m_{Z'} = 0.25$ GeV and $g_{B-L} = 10^{-6}$ the Z' proper decay length is $L_0 \sim$ cm. Accounting for an average Lorentz boost factor of about 100, the average decay length $\langle L \rangle$ can be as large as a meter. Therefore, the cuts become relevant for a small region in parameter space for our analysis.

The estimated background for this search is reported as $9.90 \pm 1.24\text{stat} \pm 1.84\text{syst}$ events for 35.9 fb^{-1} [46]. The 95% confidence level limit on the signal event rate can be derived from $\chi^2 = S^2/B > 3.84$ [50]. We have, however, used the model-independent limits given in Ref. [46]. The current sensitivity in our parameter space is obtained by requiring $\sigma_{\text{model}} < \sigma_{\text{exp}}^{\text{upper limit}}$; the limits from χ^2 are, however, very similar.

Furthermore, we also compute the reach of this analysis for High Luminosity LHC (HL-LHC) regime with 3000 fb^{-1} luminosity. As the analysis is sensitive to low mass Z', where the Z' can obtain macroscopic displacement, we implement the analysis cuts as described before and compute the HL-LHC reach with χ^2 analysis.

Z' pair production via SM Higgs at ATLAS (ATLAS $h \to 4l$). A corresponding ATLAS analysis [47] reports upper limits (U.L.) on the signal strength for pair production of light exotic bosons through decays of the SM Higgs at $\sqrt{s} = 13$ TeV with an integrated luminosity of 36.1 fb^{-1}. The analysis searches for light bosons decaying to either pair of electrons or muons; hence it searches for either $4e$, 4μ or $2e2\mu$ final states. These signal strength limits are given for the light boson decaying promptly between a mass range of 1 to 60 GeV, with the SM QCD resonance regions removed. The signal strength is the ratio of the model specific Higgs production cross section with the SM Higgs production cross section. In our model this ratio is $\cos^2\alpha$. The limits given on the signal strength hence convert to a limit on the Higgs to Z' branching ratio. We compare this to the theoretical prediction $\text{BR}^{\text{th}}(h \to Z'Z')$,

$$\begin{aligned} &\left(\frac{\sigma(h)}{\sigma(h_{\text{SM}})} \times \text{BR}(h \to Z'Z')\right)^{\text{U.L.}} \\ &= \cos^2\alpha \times \text{BR}^{\text{U.L.}}(h \to Z'Z') = \text{BR}^{\text{th}}(h \to Z'Z'). \end{aligned} \tag{4.3}$$

Unlike in the case of the CMS analysis, here we directly use the limits on the signal strength. These are derived under the assumption of a promptly decaying Z'. As discussed in Sec. III, probing small values of $g_{B-L} - Z'$ can lead to displaced vertices. Therefore, one should be careful while interpreting the limits of analyses that assume prompt final states only, as is the case here. We consider Z' to be prompt when their lab frame displacement $\langle L \rangle$ is less than 1 mm. This is fixed by inserting a prompt efficiency function $\epsilon_{\text{prompt}} \approx 1 - \exp(-1 \text{ mm}/L)$. We use the same function for the HL-LHC projections as well.

Z' final state radiation from Z production at CMS (CMS FSR). The CMS analysis [48] reports on the search for an excess in the 4μ final state when the Z' is radiated in the final state as $pp \to Z \to Z'\mu^+\mu^- \to 4\mu$ at the LHC with $\sqrt{s} = 13$ TeV with an integrated luminosity of 77.3 fb^{-1}. It considers the Z' mass range between 5 and 70 GeV. The analysis selects events with isolated muons. At least two muons are required to have $p_T > 20$ GeV, and at least one muon should have $p_T > 10$ GeV. A resonance search is then performed in pairs of oppositely charged muons. As the limits on the couplings between the two models can

easily be converted from one to another, we do not perform any special simulation. Instead, we use the limits on $L_\mu - L_\tau$ coupling $g_{L_\mu - L_\tau}$ as given by CMS. An equivalent $g_{L_\mu - L_\tau}$ can be related to g_{B-L} through $\sigma_{\text{limit}} \propto g^2_{B-L} \times \text{BR}(Z' \to \mu^+\mu^-)_{B-L} = g^2_{L_\mu - L_\tau} \text{BR}(Z' \to \mu^+\mu^-)_{L_\mu - L_\tau}$,

$$g^2_{B-L} = \frac{g^2_{L_\mu - L_\tau}}{3 \times \text{BR}(Z' \to \mu^+\mu^-)_{B-L}}, \tag{4.4}$$

because $\text{BR}(Z' \to \mu^+\mu^-)_{L_\mu - L_\tau} = 1/3$ [48]. For the HL-LHC regime, we rescale our limits. As the Z' masses considered here are more than a few GeV, no special consideration for macroscopic decay lengths are given.

Low mass Z' resonance search at CMS (CMS dilepton). Finally, we include the most recent search for a narrow low mass resonance in the dimuon final state by the CMS Collaboration [45]. This $\sqrt{s} = 13$ TeV analysis uses 96.6 fb^{-1} of data for a scouting search for a resonance between 11 and 45 GeV and the full 137 fb^{-1} Run-II reconstructed level dataset for a resonance search between 45 and 200 GeV. The analysis overcomes the traditional limitations for a dilepton resonance search in a low mass region by making use of the data scouting technique. The technique corresponds to the use of physics objects reconstructed online during data taking to perform searches and measurements. This allows for reaching low mass resonances that are otherwise difficult to search for.

The analysis interprets the results in a dark photon model and gives upper limits on the kinetic mixing ϵ as a function of dark photon mass m_{Z_D}. The limits are given in the mass range from 11.5 GeV up to 200 GeV Z_D masses. The kinetic mixing parameter ϵ is related to g_{B-L} by $g_{B-L} = e\epsilon$.

The dimuon resonance analysis is applicable to a wide range of signal models. Therefore, it is possible to constrain not just the resonance production of Z' but the Higgs mediated Z' production as well. The cross section for the Higgs mediated Z' production, however, is much smaller compared to the direct Z' production for the same g_{B-L} coupling. This is because the Higgs coupling to Z' is suppressed by both g_{B-L} and $\sin\alpha$. We therefore do not take into account the Higgs mediated process when computing the limits on g_{B-L}.

V. RESULTS

Using the above procedures for each of the existing searches, we determine the upper 95% confidence level limits on the $U(1)_{B-L}$ gauge coupling as a function of the Z' mass $m_{Z'}$. Unless stated otherwise we assume $\sin\alpha = 0.3$ for the mixing angle between the SM Higgs and the exotic scalar χ responsible for breaking the $U(1)_{B-L}$ symmetry. This assumption is, of course, crucial for the Z' pair production via the SM Higgs; for smaller values of $\sin\alpha$, the production rate is accordingly reduced and the limit on g_{B-L} is weakened.

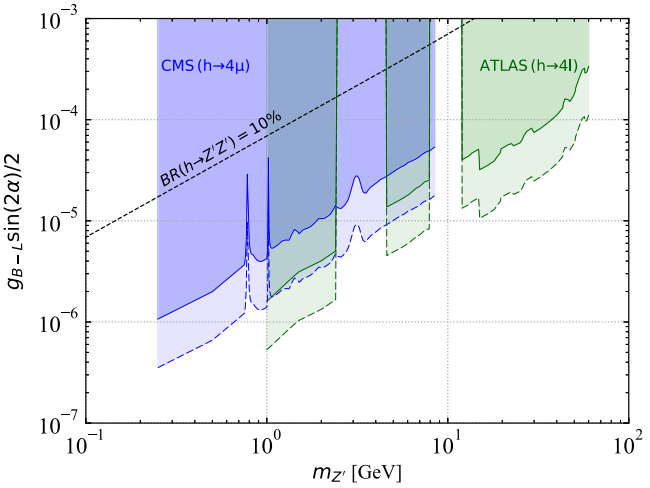

FIG. 7. Constraints on the effective coupling $g_{B-L}\sin(2\alpha)/2$ as a function of the Z' mass $m_{Z'}$ derived from the CMS $h \to 4\mu$ [46] and ATLAS $h \to 4\ell$ [47] searches. The dark colored regions are excluded by current data, whereas the light colored regions indicate the improvement expected by rescaling to a luminosity of 3,000 fb^{-1}. Also indicated is the contour for constant branching ratio $\text{BR}(h \to Z'Z') = 10\%$.

More specifically, the Higgs production cross section effectively depends on the combination $g_{B-L}\sin(2\alpha)/2$; cf. Eq. (3.1). In Fig. 7 we show the constraints from the analyses considered in this work on this parameter as a function of $m_{Z'}$. The CMS $h \to 4\mu$ constraints span an $m_{Z'}$ mass range between 0.25 and 8.5 GeV, while the ATLAS $h \to 4\ell$ cover the range between 1 and 60 GeV with two gaps between 2 2 GeV $< m_{Z'} <$ 5 GeV and 8 GeV $< m_{Z'} <$ 10.5 GeV arising from the requirement to remove QCD resonances. On the other hand, the CMS analysis estimates this background identifying correlations between dimuon invariant mass pairs. The ATLAS limits are stronger than the CMS limits where available. As can be seen from the model independent limits presented by both ATLAS and CMS, the limits on fiducial cross sections are very similar. However, the phase space in which the fiducial cross section is computed is very different. In order to demonstrate the effect of phase space we can estimate the generator level acceptance for the two analyses. For this, we implemented the acceptance cuts as given in the two analyses, and we find that the acceptance for the CMS analysis is about 25% while that for the ATLAS analysis is 50%. We also show the projections of the improved sensitivity for the high-luminosity LHC with 3,000 fb^{-1} using the lighter shaded regions delimited by a dashed curve. This projection assumes a simple scaling of signal and background with luminosity. If $h \to Z'Z'$ is the only non–Standard Model Higgs decay mode available, then it is constrained by Higgs to an invisible branching ratio. Therefore, we have also overlaid the line corresponding

to $\mathrm{BR}(h \to Z'Z') = 10\%$ which corresponds to the existing limits on Higgs to invisible branching ratio. It should be noted that strictly speaking this does not include dependence on $\cos\alpha$; however, it does depend on $\sin\alpha$ as discussed in Eq. (3.2). Furthermore, it is also worth pointing out that if heavy neutrinos are lighter than $m_h/2$, they will also contribute to this invisible BR constraint. Here we neglect the SM Higgs decaying to heavy neutrinos.

This plot is particularly useful as there is a degeneracy between g_{B-L} and $\sin\alpha$ that can only be broken by individually searching for the presence or absence of extended Higgs or gauge sectors at experiments. Using this plot, it is possible to rescale and obtain values of g_{B-L} for any value of $\sin\alpha$ desired. For example, for $m_{Z'} = 1$ GeV, at $\sin\alpha = 0.3$, $g_{B-L} \sim 3 \times 10^{-5}$, but if $\sin\alpha = 0.2$, the limit on g_{B-L} will be $\approx 5 \times 10^{-5}$. On the other hand, if we saturate the existing limits on the gauge coupling, $g_{B-L} \lesssim 10^{-4}$, the corresponding constraint on the Higgs mixing is $\sin\alpha \lesssim 0.1$. It will be difficult to independently constrain $\sin\alpha$ to such a small value by such means as direct Higgs searches. It is, however, very important to remember that such a compensation between g_{B-L} and $\sin\alpha$ is not applicable to arbitrary low values of g_{B-L}. As g_{B-L} decreases, the Z' will be longer-lived. The analyses we considered, however, largely concern themselves with prompt decays. Therefore for smaller values of g_{B-L} a simple scaling between $\sin\alpha$ and g_{B-L} will not hold true.

Apart from the two Higgs searches considered in this work, an ATLAS search in the lepton jets final state, interesting for the low mass Z' region, has been carried out at $\sqrt{s} = 8$ TeV, in both prompt [55] and displaced final states [56]. The prompt analysis is of particular interest as it targets both muon and electron jets. The displaced lepton jets analysis is not sensitive to our model as we will not have large signal cross sections and displaced Z' at the same time for a high mass region where this analysis operates. The interpretation of results in both these analyses has been done in the so-called Falkowski-Ruderman-Volansky-Zupan (FRVZ) models which have substantially different kinematics from the model considered in this work. A reinterpretation of the prompt ATLAS lepton jet analysis can be attempted; however, since it does not improve on the existing limits from 13 TeV CMS analysis considered here, we do not consider it here. Recently, ATLAS updated their search with 13 TeV data [57]; however, this analysis is not included in our work.

While Fig. 7 provides a concise summary of the Higgs mode searches, it does not accommodate search results that do not depend on $\sin\alpha$. In Fig. 8, we instead show the limits for a fixed value of $\sin\alpha = 0.3$, but we additionally show constraints from the CMS FSR and CMS dilepton searches. The constraints arising from the CMS FSR search leads to the weakest limit, $g_{B-L} \gtrsim 0.01$ for $m_{Z'}$ in the range of 5 to 60 GeV. The 4μ final state arising due to the decays of SM Higgs to a pair of Z' lead to the strongest limits between

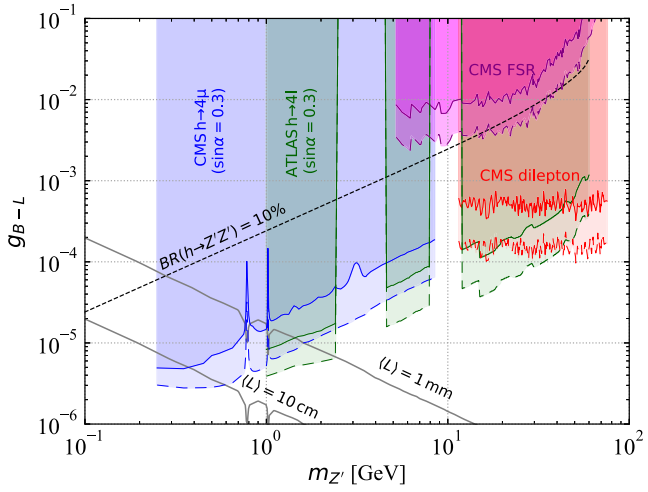

FIG. 8. Constraints on the $U(1)_{B-L}$ gauge coupling g_{B-L} as a function of the Z' mass $m_{Z'}$ derived from the CMS $h \to 4\mu$ [46], ATLAS $h \to 4\ell$ [47], CMS FSR [48], and CMS dilepton [45] searches. The dark colored regions are excluded by current data, whereas the light colored regions indicate the improvement expected by rescaling to a luminosity of $3,000\ \mathrm{fb}^{-1}$. Also indicated are the contours for constant branching ratio $\mathrm{BR}(h \to Z'Z') = 10\%$ and constant average decay length $\langle L \rangle = 1$ mm, 10 cm, the latter applicable for the Higgs mode.

$m_{Z'}$ of 0.25 to 50 GeV. Beyond $m_{Z'} = 50$ GeV, the CMS dilepton analysis leads to the strongest limits up to 70 GeV. We also denote $Z' - g_{B-L}$ values where the average lab frame Z' displacement of 1 mm and 10 cm is obtained when Z' is produced in decays of h. Finally, for reference $\mathrm{BR}(h \to Z'Z') = 10\%$ is also overlaid.

For the lowest Z' masses, the CMS $h \to 4\mu$ analysis has the strongest limits. They constrain Z' masses as low as 0.25 GeV and limit g_{B-L} to 5×10^{-6}. These limits gradually decrease to $g_{B-L} = 1.8 \times 10^{-4}$ for $m_{Z'} = 8.5$ GeV. As discussed in Sec. III, for $m_{Z'} < 1$ GeV, it is possible to gain a significant Z' displacement. This will be relevant for the High Luminosity regime. In this region of parameter space a simple scaling is not applicable. We identify the region corresponding to Z' lab decay length $\langle L \rangle$ of 1 mm and 10 cm (solid grey lines). A significant region of $m_{Z'} - g_{B-L}$ parameter space is below $\langle L \rangle = 1$ mm. As the CMS search allows for displacements up to 10 cm, it is perfectly safe to use the analysis in this region. The impact of 1 mm lab frame displacement is, however, more severe for the ATLAS search we consider as it only allows for prompt decays of the Z'. We define the prompt region to be displacements less than 1 mm. This requirement has a mild effect on the analysis efficiency; however, it is not visible in the final results. The HL-LHC reach for this analysis is correspondingly limited for low mass regions. Turning our attention to $\langle L \rangle = 10$ cm line, we see a similar picture emerge for the CMS search below $m_{Z'} < 0.5$ GeV. This is also understandable as the analysis allows for displacements up to 10 cm. In order to assess our reach for the High Luminosity reach in this

region, we have taken into account the effect of displacement. This is reflected in the limits as the gain due to luminosity is much smaller in the displaced region $m_{Z'} \lesssim 0.5$ GeV compared to the prompt region $m_{Z'} \gtrsim 0.5$ GeV. The same can be seen for the ATLAS search.

Finally, we also show recent limits on the dimuon final state resonance search using the data scouting technique as presented by the CMS Collaboration [45]. This limit improves on the previous LHCb limit for a resonance search in the same final state from the mass range of 11.5 GeV and presents competitive limits from the Higgs to four-lepton final state in the mass range between 10 and 50 GeV. In the mass range of 50 to 70 GeV, this analysis has the best limits on g_{B-L}.

Of particular interest is also the behavior of limits from the FSR and dilepton final state against those from the Higgs mediated four-lepton final state. The limits on the g_{B-L} from the FSR and dilepton final states are approximately constant over a wide range of Z' mass. The limits on g_{B-L} coming from the Higgs mediated processes, however, sharply degrade as $m_{Z'}$ increases. This is because the four-lepton final state cross section is dominantly controlled by the branching ratio of the SM-like Higgs decays to the Z' pairs, which depends on $g_{B-L}/m_{Z'}$ according to Eqs. (3.2) and (3.1).

Given our discussion so far, it is clear that it will be difficult to probe large Z' displacements in the $B-L$ model unlike in the dark photon case. However, the above discussion is built based on the assumption that we neglect the $Z-Z'$ mixing of the $B-L$ model. If this mixing is opened, complex interactions will be introduced as the $B-L$ sector can now couple to the SM particles via both the hypercharge portal and the $B-L$ charge. The relative strength of the two couplings g_{B-L} and $\tilde{g}$ will then control the behavior of the limits.

VI. CONCLUSIONS

In this work, we have considered the impact of LHC searches on the parameters of the minimal $B-L$ model for Z' masses in the region ≈0.2 GeV to 200 GeV. The minimal $B-L$ can be considered as the simplest gauge realization to generate the light neutrino masses via a type-I seesaw mechanism and probing it will help in our understanding of neutrinos. The model presents a distinctly different phenomenology compared to the popular dark photon models. For example, unlike the dark photon models, the production and decay of $B-L$ Z' are controlled by the same parameters, which limits the sensitivity of LHC searches due to rapidly falling cross sections.

We have mainly explored three different Z' production mechanisms at the LHC. The Z' can be produced either via s-channel Drell-Yan, decays of the SM Higgs, or via the final state radiation of the muons produced in the SM Drell-Yan process at the LHC. We demonstrated that the limits from the final state radiation arising from [48] are the weakest. As for the four-lepton final states produced via the SM Higgs we showed that the limits from existing searches are sensitive to the macroscopic Z' displacements at the LHC. These searches have a potential to constrain large regions of $m_{Z'} - g_{B-L}$ parameter space and are particularly powerful for light Z' masses. The constraints from the ATLAS search [40] are somewhat stronger than the CMS search [58] as ATLAS takes into account Z' decays to both electrons and muon final state. On the other hand, the CMS search covers a wider $m_{Z'}$ interval. The Higgs production mode depends on the Higgs mixing angle $\sin\alpha$. In our analysis we have chosen a representative, approximately maximal value (given current limits) of $\sin\alpha = 0.3$. For smaller values the sensitivity to g_{B-L} will accordingly weaken but our results illustrate the interplay of parameters in a realistic gauge model and the potential sensitivity to small exotic gauge couplings at the LHC. The four-lepton final state searches are further complemented by searches for dileptons. The most recent scouting analysis of the CMS dimuon search [45] presents competitive limits in the mass range of 10 to 60 GeV.

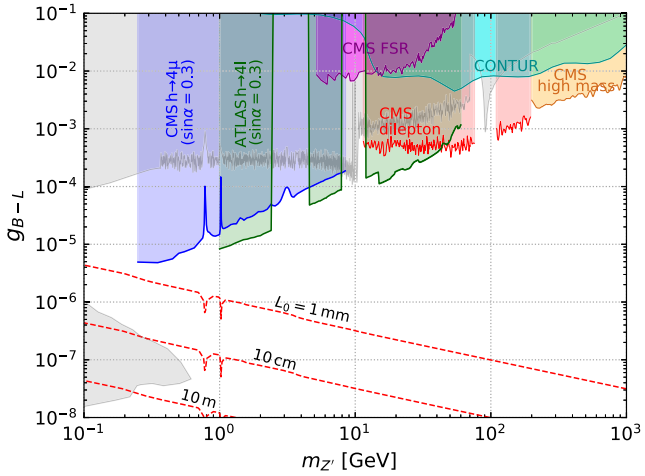

FIG. 9. Summary of constraints on the $U(1)_{B-L}$ gauge coupling g_{B-L} as a function of the Z' mass $m_{Z'}$. The grey area represents existing constraints, whereas the colored regions represent the new constraints obtained in this paper derived from the CMS $h \to 4\mu$ [46], ATLAS $h \to 4\ell$ [47], CMS FSR [48], and CMS dilepton [45] searches. Also shown are the constraints derived from the CMS dilepton search [58] (CMS high mass) and from the LHC SM measurements using CONTUR [14] (CONTUR). For the Higgs mediated modes we assume a Higgs mixing angle $\sin\alpha = 0.3$.

The summary of our results is presented in Fig. 9. The plot also contains previously known limits on Z' masses. In the mass region of 0.25–1 GeV our analysis shows that there is a sensitivity improvement to probe Z' limits by an order of magnitude. In the mass region between 10 and 60 GeV, the Higgs mediated channel and the recent CMS dilepton search in the dimuon final state also improve on the existing limits. Finally, for completeness, we also derive

limits by interpreting recent high mass dilepton resonance searches. For this purpose, we use results from the most recent CMS high mass dilepton search [58]. This analysis presents limits on the ratio of the dilepton resonance cross section to the SM Z to dilepton production cross section. Taking the Z to muon cross section to be 1870 pb, we derive limits on g_{B-L}. We have checked that the corresponding ATLAS analysis [40] yields similar limits. It should be noted that the limits from high mass resonance searches constrain masses well beyond 1 TeV. The figure also illustrates the gaps in the dilepton resonance searches at ATLAS and CMS. In the region around $m_{Z'}$ of 10 GeV, only weak constraints from the CMS FSR analysis can be derived, while the region around the Z mass remains unconstrained by current LHC searches. As discussed in [14], using the constraints on new theories using Rivet (CONTUR) method of interpreting LHC SM measurements can still be used to extract constraints, albeit comparatively weaker. The resulting limits on g_{B-L} are indicated in Fig. 9.

The ultimate prize when probing models such as the minimal $U(1)_{B-L}$ is to unravel the mechanism of neutrino mass generation. In our case this corresponds to discovering the heavy Majorana neutrinos giving rise to the seesaw mechanism. Because the heavy neutrinos are charged under the $U(1)_{B-L}$ gauge group, they can be produced not only via their mixing with the active neutrinos, which is generically expected to be small to explain the lightness of neutrinos, but also via the Z', the $U(1)_{B-L}$ breaking Higgs χ, and the SM Higgs (due to Higgs mixing). We here focus on the production of the Z' at the LHC in the minimal $B-L$ models. Other aspects of $B-L$ models were discussed elsewhere. For example, a $B-L$ model with a specific low scale seesaw mechanism is discussed in Ref. [59], with an inverse seesaw scenario in Ref. [60] and with a linear seesaw scenario in Ref. [61]. Other aspects of heavy neutrinos were, for example, discussed in Refs. [62–66], including displaced vertex signatures. Finally, dark matter can be incorporated in $B-L$ models as well as has been, for example, discussed in Refs. [67–70].

The SM Higgs and Z' channels were recently discussed in [51,71–73]. The vertex coupling the hNN (SM Higgs) is proportional to $m_N/m_{Z'} \times \sin\alpha g_{B-L}$, whereas the $Z'NN$ vertex is proportional to g_{B-L}. From our analysis, we can thus infer new limits on the heavy neutrino production modes. As shown in Fig. 8, when the Z' production via Higgs is feasible, we obtain a conservative limit of $g_{B-L} < 10^{-4}$ for Z' masses between 10 to 60 GeV. For lower masses of Z' the limits get even more constraining. With this revised constraint on the Z' coupling the heavy neutrino production via both channels is therefore suppressed and is not expected to yield a detectable cross section. Likewise, the branching ratio $\mathrm{BR}(h \to NN)$ depends on $m_{Z'}/g_{B-L}$. For $m_{Z'} < 100$ GeV and when applying our constraints this ratio is $\approx$100 TeV. This is about 30 times larger than the value considered in Ref. [51], resulting in about a thousand times smaller cross section. Heavy neutrino production from Z' decays mentioned in Ref. [71] is suppressed as well due to roughly a magnitude better constraint on g_{B-L} which makes the Z' production cross section a hundred times smaller. This, of course, applies to the case where the Higgs mixing is near its maximally allowed value, $\sin\alpha \approx 0.3$, and the discussion will change for smaller values; in such a case the heavy neutrino Higgs portal $pp \to h \to NN$ will be suppressed though. With $\mathrm{BR}(Z' \to NN) \approx 6\%$, the largest $pp \to Z' \to NN$ cross section is only several femtobarn for a narrow range of Z' masses between 10 and 15 GeV. One can also consider heavy neutrinos in cascade decays such as $pp \to h \to Z'Z' \to NN + X$. With $\sigma(pp \to h \to Z'Z') \approx 1$ fb and $\mathrm{BR}(Z' \to NN) \times \mathrm{BR}(N \to \mu + X) \approx 1\%$ for $g_{B-L} \approx 10^{-5}$ and $m_{Z'} > 1$ GeV, the total cross section of this process amounts to 10^{-2} fb.

These considerations demonstrate that with the updated limits considered in this work, there is very little room for producing heavy neutrinos with long decay lengths (heavy neutrinos with shorter decay lengths can still be searched for via W and Z decays). It may still be possible to gain some sensitivity in this channel for the High Luminosity LHC. With these considerations we merely like to point out the importance of searching not only for heavy neutral leptons (i.e., heavy neutrinos) but also for the potential exotic mediators and portals through which they can be produced. This will shed light on whether the light neutrino masses have their origin in new physics around the TeV scale.

ACKNOWLEDGMENTS

W. L. acknowledges support via the China Scholarship Council (Grant CSC No. 2016 08060325). S. K. is supported by Elise-Richter Grant Project No. V592-N27 of the Austrian Science Fund. F. F. D. by a UK STFC consolidated grant (Reference ST/P00072X/1). We thank Alberto Escalante del Valle and Ivan Mikulec (CMS) for several useful discussions Austrian Science Fund.

[1] R. N. Mohapatra and J. W. F. Valle, Neutrino mass and baryon number nonconservation in superstring models, Phys. Rev. D **34**, 1642 (1986).

[2] A. Davidson, $B^{-}1$ as the fourth color, quark—lepton correspondence, and natural masslessness of neutrinos within a generalized ws model, Phys. Rev. D **20**, 776 (1979).

[3] R. N. Mohapatra and R. E. Marshak, Local $B-L$ Symmetry of Electroweak Interactions, Majorana Neutrinos and Neutron Oscillations, Phys. Rev. Lett. **44**, 1316 (1980).

[4] M. Aaboud *et al.* (ATLAS Collaboration), Search for new high-mass phenomena in the dilepton final state using 36 fb^{-1} of proton-proton collision data at $\sqrt{s}=13$ TeV with the ATLAS detector, J. High Energy Phys. 10 (2017) 182.

[5] SLD Electroweak Group, SLD Heavy Flavor Group, DELPHI, LEP, ALEPH, OPAL, LEP Electroweak Working Group, L3 collaboration, t. S. Electroweak, A Combination of preliminary electroweak measurements and constraints on the standard model, arXiv:hep-ex/0312023.

[6] P. L. Anthony *et al.* (SLAC E158 Collaboration), Observation of Parity Nonconservation in Moller Scattering, Phys. Rev. Lett. **92**, 181602 (2004).

[7] M. Carena, A. Daleo, B. A. Dobrescu, and T. M. P. Tait, Z' gauge bosons at the Tevatron, Phys. Rev. D **70**, 093009 (2004).

[8] G. Cacciapaglia, C. Csaki, G. Marandella, and A. Strumia, The minimal set of electroweak precision parameters, Phys. Rev. D **74**, 033011 (2006).

[9] R. Harnik, J. Kopp, and P. A. N. Machado, Exploring nu signals in dark matter detectors, J. Cosmol. Astropart. Phys. 07 (2012) 026.

[10] G. Bellini *et al.*, Precision Measurement of the 7Be Solar Neutrino Interaction Rate in Borexino, Phys. Rev. Lett. **107**, 141302 (2011).

[11] M. Bauer, P. Foldenauer, and J. Jaeckel, Hunting all the hidden photons, J. High Energy Phys. 07 (2018) 094.

[12] P. Vilain *et al.* (CHARM-II Collaboration), Measurement of differential cross-sections for muon-neutrino electron scattering, Phys. Lett. B **302**, 351 (1993).

[13] M. Deniz *et al.* (TEXONO Collaboration), Measurement of Nu(e)-bar -electron scattering cross-section with a CsI(Tl) scintillating crystal array at the Kuo-Sheng nuclear power reactor, Phys. Rev. D **81**, 072001 (2010).

[14] S. Amrith, J. M. Butterworth, F. F. Deppisch, W. Liu, A. Varma, and D. Yallup, LHC constraints on a $B-L$ gauge model using contur, J. High Energy Phys. 05 (2019) 154.

[15] J. M. Butterworth, D. Grellscheid, M. Krämer, B. Sarrazin, and D. Yallup, Constraining new physics with collider measurements of Standard Model signatures, J. High Energy Phys. 03 (2017) 078.

[16] P. Ilten, Y. Soreq, M. Williams, and W. Xue, Serendipity in dark photon searches, J. High Energy Phys. 06 (2018) 004.

[17] R. Aaij *et al.* (LHCb Collaboration), Search for Dark Photons Produced in 13 TeV pp Collisions, Phys. Rev. Lett. **120**, 061801 (2018).

[18] P. Bechtle, S. Heinemeyer, O. Stal, T. Stefaniak, and G. Weiglein, *HiggsSignals*: Confronting arbitrary Higgs sectors with measurements at the Tevatron and the LHC, Eur. Phys. J. C **74**, 2711 (2014).

[19] A. Ilnicka, T. Robens, and T. Stefaniak, Constraining extended scalar sectors at the LHC and beyond, Mod. Phys. Lett. A **33**, 1830007 (2018).

[20] P. Bechtle, S. Heinemeyer, O. Stal, T. Stefaniak, and G. Weiglein, Probing the Standard Model with Higgs signal rates from the Tevatron, the LHC and a future ILC, J. High Energy Phys. 11 (2014) 039.

[21] ATLAS Collaboration, Measurements of the Higgs boson production cross section via Vector Boson Fusion and associated WH production in the $WW^{*}\to\ell\nu\ell\nu$ decay mode with the ATLAS detector at $\sqrt{s}=13$ TeV, Report No. ATLAS-CONF-2016-112, 2016.

[22] ATLAS Collaboration, Study of the Higgs boson properties and search for high-mass scalar resonances in the $H\to ZZ^{*}\to 4\ell$ decay channel at $\sqrt{s}=13$ TeV with the ATLAS detector, Report No. ATLAS-CONF-2016-079, 2016.

[23] ATLAS Collaboration, Search for the Standard Model Higgs boson produced in association with a vector boson and decaying to a $b\bar{b}$ pair in pp collisions at 13 TeV using the ATLAS detector, Report No. ATLAS-CONF-2016-091, 2016.

[24] ATLAS Collaboration, Search for the Standard Model Higgs boson produced in association with top quarks and decaying into $b\bar{b}$ in pp collisions at $\sqrt{s}=13$ TeV with the ATLAS detector, Report No. ATLAS-CONF-2016-080, 2016.

[25] ATLAS Collaboration, Measurement of fiducial, differential and production cross sections in the $H\to\gamma\gamma$ decay channel with 13.3 fb^{-1} of 13 TeV proton-proton collision data with the ATLAS detector, Report No. ATLAS-CONF-2016-067, 2016.

[26] ATLAS Collaboration, Search for the Associated Production of a Higgs Boson and a Top Quark Pair in Multilepton Final States with the ATLAS Detector, Report No. ATLAS-CONF-2016-058, 2016.

[27] A. M. Sirunyan *et al.* (CMS Collaboration), Measurements of properties of the Higgs boson decaying into the four-lepton final state in pp collisions at $\sqrt{s}=13$ TeV, J. High Energy Phys. 11 (2017) 047.

[28] CMS Collaboration, Updated measurements of Higgs boson production in the diphoton decay channel at $\sqrt{s}=13$ TeV in pp collisions at CMS, Report No. CMS-PAS-HIG-16-020, 2016.

[29] CMS Collaboration, Combination of standard model Higgs boson searches and measurements of the properties of the new boson with a mass near 125 GeV, Report No. CMS-PAS-HIG-12-045, 2016.

[30] CMS Collaboration, Update on the search for the standard model Higgs boson in pp collisions at the LHC decaying to $W+W$ in the fully leptonic final state, Report No. CMS-PAS-HIG-13-003, 2013.

[31] V. Khachatryan *et al.* (CMS Collaboration), Search for a Higgs boson in the mass range from 145 to 1000 GeV decaying to a pair of W or Z bosons, J. High Energy Phys. 10 (2015) 144.

[32] CMS Collaboration Search for a new scalar resonance decaying to a pair of Z bosons in proton-proton collisions at $\sqrt{s}=13$ TeV, Report No. CMS-PAS-HIG-17-012, 2017.

[33] M. Aaboud *et al.* (ATLAS Collaboration), Search for heavy ZZ resonances in the $\ell^+\ell^-\ell^+\ell^-$ and $\ell^+\ell^-\nu\bar{\nu}$ final states using proton–proton collisions at $\sqrt{s} = 13$ TeV with the ATLAS detector, Eur. Phys. J. C **78**, 293 (2018).

[34] D. Lopez-Val and T. Robens, Δr and the W-boson mass in the singlet extension of the standard model, Phys. Rev. D **90**, 114018 (2014).

[35] T. Robens and T. Stefaniak, Status of the higgs singlet extension of the standard model after LHC run 1, Eur. Phys. J. C **75**, 104 (2015).

[36] F. D'Eramo, B. J. Kavanagh, and P. Panci, Probing leptophilic dark sectors with hadronic processes, Phys. Lett. B **771**, 339 (2017).

[37] A. Anastasi *et al.*, Limit on the production of a low-mass vector boson in $e^+e^- \to U\gamma$, $U \to e^+e^-$ with the KLOE experiment, Phys. Lett. B **750**, 633 (2015).

[38] J. P. Lees *et al.* (*BABAR* Collaboration), Search for a Dark Photon in e^+e^- Collisions at *BABAR*, Phys. Rev. Lett. **113**, 201801 (2014).

[39] A. M. Sirunyan *et al.* (CMS Collaboration), Search for high-mass resonances in dilepton final states in proton-proton collisions at $\sqrt{s} = 13$ TeV, J. High Energy Phys. 06 (2018) 120.

[40] G. Aad *et al.* (ATLAS Collaboration), Search for high-mass dilepton resonances using 139 fb^{-1} of pp collision data collected at $\sqrt{s} = 13$ TeV with the ATLAS detector, Phys. Lett. B **796**, 68 (2019).

[41] A. M. Sirunyan *et al.* (CMS Collaboration), Search for low-mass quark-antiquark resonances produced in association with a photon at $\sqrt{s} = 13$ TeV, arXiv:1905.10331.

[42] J. Gu, H. Li, Z. Liu, S. Su, and W. Su, Learning from higgs physics at future higgs factories, J. High Energy Phys. 12 (2017) 153.

[43] M. Dong *et al.* (CEPC Study Group Collaboration), CEPC conceptual design report: Volume 2—Physics & Detector, arXiv:1811.10545.

[44] T. Fujiwara, T. Kugo, H. Terao, S. Uehara, and K. Yamawaki, Nonabelian anomaly and vector mesons as dynamical gauge bosons of hidden local symmetries, Prog. Theor. Phys. **73**, 926 (1985).

[45] CMS Collaboration, Search for a narrow resonance decaying to a pair of muons in proton-proton collisions at 13 TeV, Tech. Rep. CMS-PAS-EXO-19-018, CERN, Geneva, 2019.

[46] A. M. Sirunyan *et al.* (CMS Collaboration), A search for pair production of new light bosons decaying into muons in proton-proton collisions at 13 TeV, Phys. Lett. B **796**, 131 (2019).

[47] M. Aaboud *et al.* (ATLAS Collaboration), Search for Higgs boson decays to beyond-the-Standard-Model light bosons in four-lepton events with the ATLAS detector at $\sqrt{s} = 13$ TeV, J. High Energy Phys. 06 (2018) 166.

[48] A. M. Sirunyan *et al.* (CMS Collaboration), Search for an $L_\mu - L_\tau$ gauge boson using $Z \to 4\mu$ events in proton-proton collisions at $\sqrt{s} = 13$ TeV, Phys. Lett. B **792**, 345 (2019).

[49] D. de Florian *et al.* (LHC Higgs Cross Section Working Group Collaboration), Handbook of LHC higgs cross sections: 4. Deciphering the nature of the higgs sector, arXiv:1610.07922.

[50] M. Tanabashi *et al.* (Particle Data Group Collaboration), Review of particle physics, Phys. Rev. D **98**, 030001 (2018).

[51] F. F. Deppisch, W. Liu, and M. Mitra, Long-lived heavy neutrinos from higgs decays, J. High Energy Phys. 08 (2018) 181.

[52] C. Degrande, C. Duhr, B. Fuks, D. Grellscheid, O. Mattelaer, and T. Reiter, UFO—The universal FeynRules output, Comput. Phys. Commun. **183**, 1201 (2012).

[53] J. Alwall, R. Frederix, S. Frixione, V. Hirschi, F. Maltoni, O. Mattelaer, H.-S. Shao, T. Stelzer, P. Torrielli, and M. Zaro, The automated computation of tree-level and next-to-leading order differential cross sections, and their matching to parton shower simulations, J. High Energy Phys. 07 (2014) 079.

[54] T. Sjöstrand, S. Ask, J. R. Christiansen, R. Corke, N. Desai, P. Ilten, S. Mrenna, S. Prestel, C. O. Rasmussen, and P. Z. Skands, An introduction to PYTHIA 8.2, Comput. Phys. Commun. **191**, 159 (2015).

[55] G. Aad *et al.* (ATLAS Collaboration), A search for prompt lepton-jets in pp collisions at $\sqrt{s} = 8$ TeV with the ATLAS detector, J. High Energy Phys. 02 (2016) 062.

[56] G. Aad *et al.* (ATLAS Collaboration), Search for long-lived neutral particles decaying into lepton jets in proton-proton collisions at $\sqrt{s} = 8$ TeV with the ATLAS detector, J. High Energy Phys. 11 (2014) 088.

[57] G. Aad *et al.* (ATLAS Collaboration), Search for light long-lived neutral particles produced in pp collisions at $\sqrt{s} = 13$ TeV and decaying into collimated leptons or light hadrons with the ATLAS detector, arXiv:1909.01246.

[58] CMS Collaboration, Search for a narrow resonance in high-mass dilepton final states in proton-proton collisions using 140 fb^{-1} of data at $\sqrt{s} = 13$ TeV, Tech. Rep. CMS-PAS-EXO-19-019, CERN, Geneva, 2019.

[59] S. Khalil, Low scale B-L extension of the Standard Model at the LHC, J. Phys. G **35**, 055001 (2008).

[60] S. Khalil, TeV-scale gauged $B - L$ symmetry with inverse seesaw mechanism, Phys. Rev. D **82**, 077702 (2010).

[61] C. O. Dib, G. R. Moreno, and N. A. Neill, Neutrinos with a linear seesaw mechanism in a scenario of gauged $B - L$ symmetry, Phys. Rev. D **90**, 113003 (2014).

[62] A. Das, N. Okada, and D. Raut, Enhanced pair production of heavy Majorana neutrinos at the LHC, Phys. Rev. D **97**, 115023 (2018).

[63] A. Das, N. Okada, and D. Raut, Heavy Majorana neutrino pair productions at the LHC in minimal U(1) extended Standard Model, Eur. Phys. J. C **78**, 696 (2018).

[64] E. J. Chun, A. Das, J. Kim, and J. Kim, Searching for flavored gauge bosons, J. High Energy Phys. 02 (2019) 093.

[65] A. Das, N. Okada, S. Okada, and D. Raut, Probing the seesaw mechanism at the 250 GeV ILC, Phys. Lett. B **797**, 134849 (2019).

[66] S. Jana, N. Okada, and D. Raut, Displaced vertex signature of type-I seesaw model, Phys. Rev. D **98**, 035023 (2018).

[67] M. Klasen, F. Lyonnet, and F. S. Queiroz, NLO + NLL collider bounds, Dirac fermion and scalar dark matter in the B–L model, Eur. Phys. J. C **77**, 348 (2017).

[68] P. Fileviez Pérez, C. Murgui, and A. D. Plascencia, Neutrino-dark matter connections in gauge theories, Phys. Rev. D **100**, 035041 (2019).

[69] S. Heeba and F. Kahlhoefer, Probing the freeze-in mechanism in dark matter models with $U(1)'$ gauge extensions, arXiv:1908.09834.

[70] R. N. Mohapatra and N. Okada, Dark matter constraints on low mass and weakly coupled $B - L$ gauge boson, arXiv:1908.11325.

[71] F. Deppisch, S. Kulkarni, and W. Liu, Heavy neutrino production via Z' at the lifetime frontier, Phys. Rev. D **100**, 035005 (2019).

[72] A. Das, P. S. B. Dev, and N. Okada, Long-lived TeV-scale right-handed neutrino production at the LHC in gauged $U(1)_X$ model, Phys. Lett. B **799**, 135052 (2019).

[73] C.-W. Chiang, G. Cottin, A. Das, and S. Mandal, Displaced heavy neutrinos from Z' decays at the LHC, arXiv:1908.09838.